Robotica (2004) volume 22, pp. 599–609. © 2004 Cambridge University Press
DOI: 10.1017/S0263574704000396 Printed in the United Kingdom

# Optimal design of a micro parallel positioning platform. Part I: Kinematic analysis

Kun-Ku Oh, Xin-Jun Liu, Deuk Soo Kang and Jongwon Kim*

*School of Mechanical and Aerospace Engineering, Seoul National University, Seoul 151-744 (Republic of Korea)*

(Received in Final Form: March 8, 2004)

**SUMMARY**

Using a coarse-and-fine actuator combination (dual stage system), a new design of the three degree-of-freedom (DOF) micro parallel positioning platform with high mobility, high accuracy, and a large working space is proposed. To achieve these three DOFs and implement the dual stage system, there are six possible architectures for the coarse and fine actuators, respectively. This paper is organized in two parts. Part I treats the kinematic analysis of each architecture and the problem of selecting the correct coarse actuator architecture. Inverse kinematics and Jacobian matrices for six types of coarse actuator architectures are derived and one proper coarse actuator architecture is selected based on the mobility (rotational capability) analysis, condition number evaluation of the Jacobian matrix, and manufacturability consideration. Part II on real machine design will follow in the next issue of *Robotica*.

KEYWORDS: Parallel mechanism; Micro positioning platform; Dual stage system; Kinematics

## 1. INTRODUCTION

Recent developments in the fields of microstructures, micro-mechanical devices, microelectronics and optics require components of complex three-dimensional shape from a few millimeters to sub millimeters with high accuracy to be applied to devices such as micro robots, micro actuators, micro sensors, micro pumps, etc. Even though the sizes of these components are getting smaller and smaller, they are usually manufactured in the traditional clean-rooms or by full-sized conventional manufacturing systems such as the CNC milling machines or EDM (Electro Discharge Machining) machines. Larger manufacturing systems require larger space and larger energy consumption. Thus, the demands for miniaturized manufacturing systems have been growing for space savings, energy savings, easy transportation, and less environment problems.[1]

On the other hand, to manufacture, assemble or manipulate these three-dimensional precise components, a positioning devices with sub-micron accuracy and high mobility (rotational capability) over a large working space is needed. A common method to achieve sub-micron accuracy involves the use of a stage with piezoelectric fine actuators and wire-EDM-cut flexures. However, these fine actuators have usually less than 100 microns of motion range and show no or little spatial rotational capability. One of the practical methods to achieve sub-micron accuracy in a large working space is to use the dual stage system with the coarse and fine actuators. The coarse actuator offers a large working space and actuation powers, while the fine actuator enables high resolution of motion.

Serial mechanisms with a dual stage system are used mostly in these applications.[2–4] Such serial mechanisms suffer from their low speed and residual vibration due to their large moving mass. Parallel mechanisms can be an alternative solution because they can be modularized, have actuators fixed to the base, are light, have high motion dynamics and accuracy combined with high structural rigidity due to their closed kinematic loops.[5,6]

Most of the parallel mechanisms are six-strut platforms with six DOFs, called the Stewart-Gough platform. These mechanisms are popular in diverse applications such as motion simulators, machine tools, virtual reality games, positioning device, measuring device, haptic device, and medical device.[7] However, they suffer from poor ratio of system size to workspace, pose dependent performance, more complex control, and design difficulties. Furthermore, their forward kinematics involves many different problems (the solutions are not unique, and the solution procedures are time consuming and complicated for practical applications.) and their mobility is limited due to multi-closed chains and limited motion range of spherical joints. For such reason, researchers have been increasingly drawn to parallel mechanisms with less than six DOFs. Parallel mechanisms have been also applied to the field of micro machines. But most of these mechanisms are micro positioning devices with low rotational capability (mobility), in which flexure joints are adopted.[8,9] Mobility is undoubtedly one of the most important requirements in some applications such as micro-fabrication and micro-manipulation.

Y. Takeda *et al.*[10] presented a 6-DOF parallel mechanism for fine positioning with a large working space by using a coarse-and-fine actuator combination. There are several possibilities for the location of the coarse and fine actuators in the parallel mechanism. They considered four possible combinations and selected one coarse-and-fine actuator combination among them. But their prototype machine is somewhat large (540 mm × 540 mm × 500 mm) so it cannot be called a miniaturized manufacturing system. And, the prototype machine has the mobility of $\pm 10^{\circ}$ because of the Stewart-Gough platform, which acts as a basic mechanism.

* Corresponding author. E-mail address: jongkim@snu.ac.kr

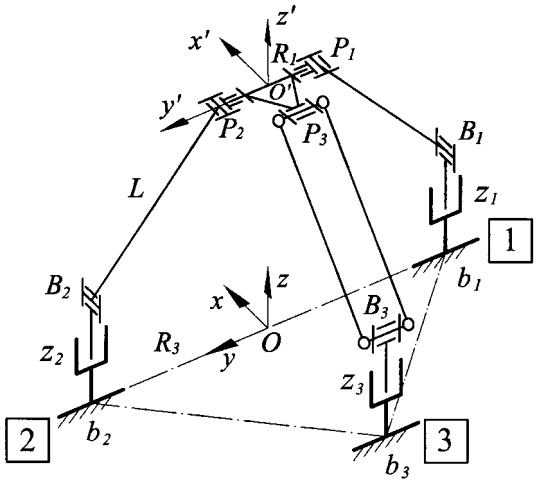


*O-xyz*: Fixed global reference frame

*O'-x'y'z'*: Movable top frame

$P_1$, $P_2$, $P_3$: Movable Platform joints

$B_1$, $B_2$, $B_3$: Base joints

$b_1$, $b_2$, $b_3$ : Vertices of base plate

$L$ or ($P_iB_i$): Length of link for each leg

$R_1$ or ($O'P_i$): Radius of moving platform

$R_3$ or ($Ob_i$): Radius of base plate

$Z_1$, $Z_2$, $Z_3$ : Actuator inputs

Fig. 1. A kinematic model of the 3-DOF parallel mechanism.

This paper proposes a new design for the micro parallel positioning platform with high mobility and high accuracy by using a dual stage system to realize the concepts of a miniaturized manufacturing system and sub-micron accuracy with a large working space. The target specifications for the overall size and working space of the micro parallel positioning platform are less than 50 mm × 50 mm × 50 mm and more than $\phi$5 mm × height 5 mm with 100° mobility, respectively. The positioning platform is based on a new spatial 3-DOF parallel mechanism which has a distinct advantage in high mobility.[11] The movable platform of the mechanism has three DOFs, which are two degrees of translational freedom and one degree of rotational freedom with respect to the base. To achieve these three DOFs and implement the dual stage system, there are six possible architectures for the coarse and fine actuators, respectively. Thus, the total number of possible coarse-and-fine actuator combinations is 36. The problem of selecting the proper coarse-and-fine actuator combination among 36 candidates occurs at the design stage.

In part I of this paper, inverse kinematics and Jacobian matrices for six types of coarse actuator architectures are derived, and each type of coarse actuator architecture is evaluated by the criteria of the rotational capability of the platform, better condition number of the Jacobian matrix, and manufacturability consideration to determine one proper coarse actuator architecture. In part II (next issue of the journal) an optimal kinematic parameter set is determined for the selected coarse actuator architecture, and one fine actuator architecture among six possible fine actuator architectures is selected to achieve sub-micron positioning accuracy.

## 2. DESCRIPTION OF THE MECHANISM

The 3-DOF parallel mechanism consists of a base plate, a movable platform, and three legs that connect the aforementioned two plates. A kinematics model of the manipulator is shown as in Fig. 1. Vertices of the output platform are denoted as platform joints $P_i$ ($i = 1, 2, 3$), and vertices of the base plate denoted as $b_i$ ($i = 1, 2, 3$). A fixed global reference frame $\Re$:*O-xyz* is located at the center of the side $b_1b_2$ with the $z$-axis normal to the base plate and the $y$-axis directed along $b_1b_2$. Another reference frame, called the top frame $\Re'$: $O'$-$x'y'z'$, is located at the center of the side $P_1P_2$. The $z'$-axis is perpendicular to the output platform and $y'$-axis directed along $P_1P_2$. The length of the link for each leg is denoted as $L$, where $P_iB_i = L$ ($i = 1, 2, 3$). The platform is an isosceles triangle described by its parameter $R_1$, where $O'P_i = R_1$ ($i = 1, 2, 3$). Parameter $R_3$ designates the size of the base plate, that is $Ob_i = R_3$ ($i = 1, 2, 3$).

The first and second legs have identical chains, each of which consists of a link connected to the moving platform by a universal joint (or two revolute joints), and to the base through a passive revolute joint. For actuating each of the two legs, the slider can be attached to the base by an active prismatic joint in the vertical or horizontal direction or it is also possible to make a variable link by attaching an active prismatic joint in the link. The first and second legs provide two constraints on the rotation of the moving platform about the $z$-axis and the translation along $x$-axis.

The third leg is very different from the two legs, in which a planar four-bar parallelogram is connected to the moving platform with a passive revolute joint, and to the base by another passive revolute joint. For actuating the leg, the slider can be also attached to the base by an active prismatic joint in the vertical or horizontal direction. The two revolute joints for the third leg have parallel axes as shown in Fig. 1. The leg can provide two constraints on the rotation of the moving platform about $x$ and $z$-axes.

Hence, the combination of the three legs constrains the rotation of the moving platform with respect to $x$ and $z$-axes and the translation along $x$-axis. This leaves the mechanism with two translational degrees in $O$-$yz$ plane and one rotational DOF about $y$-axis. One of the distinct advantages of the parallel mechanism is that the rotational DOF has high mobility, which makes it very different in design from other parallel mechanisms. Because of the swift design of this mechanism, two translational degrees in $O$-$yz$ plane are achieved mainly by the movement of the first and second legs and the rotational DOF about $y$-axis is achieved mainly by the movement of the third leg.

https://doi.org/10.1017/S0263574704000396 Published online by Cambridge University Press

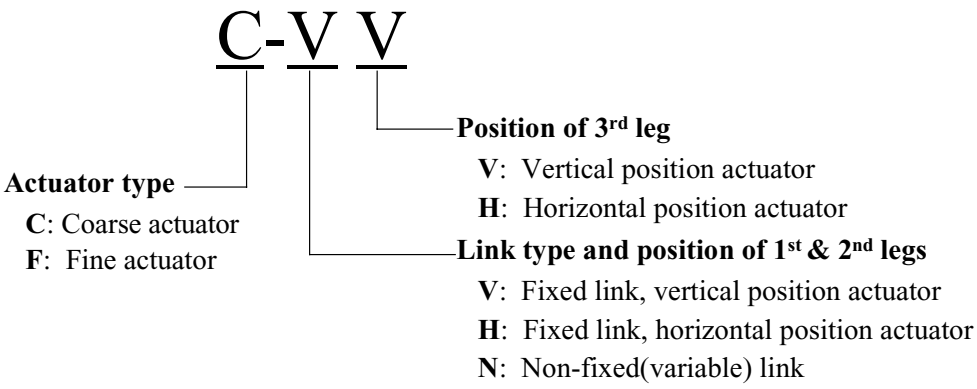


Fig. 2. Nomenclature for differentiating each architecture.

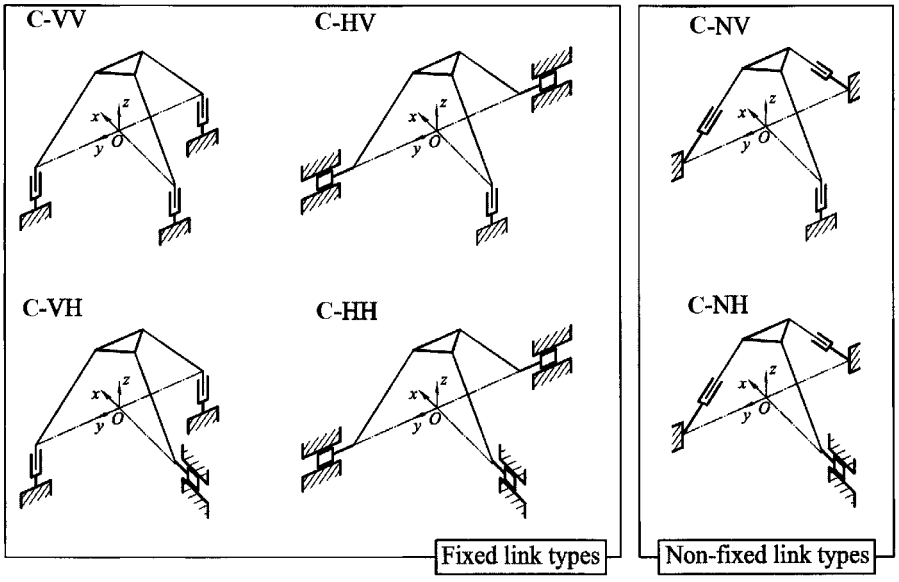


Fig. 3. Six possible architectures with coarse actuators.

This parallel mechanism will be applied to the micro parallel positioning platform that is being developed at Robust Design Engineering Laboratory in Seoul National University. The concept of the micro parallel positioning platform will be discussed in section 4 of part II. The target specifications for the overall size and working space of micro parallel positioning platform are less than 50 mm × 50 mm × 50 mm and more than $\phi$5 mm × height 5 mm with 100° mobility, respectively. The positioning platform will be used to make 3D micro mechanical components whose lengths are from 0.01 mm to 5 mm with sub-micron accuracy.

To achieve sub-micron accuracy with a large working space, we are going to use the dual stage system with the coarse and fine actuators. There are several possible architectures for the locations of the coarse and fine actuators in the parallel mechanism. For the symmetry reason, the first and second legs must have the same actuator locations. Then the possible architectures for the first and second legs are 1) fixed links and horizontal locations of the actuators (H type), 2) fixed links and vertical locations of the actuators (V type), and 3) variable (non-fixed) links with the active prismatic actuators (N type). For the third leg that has a planar four-bar parallelogram, only the architectures of the fixed link with the horizontal (H type) or vertical (V type) location of the actuator are possible.

Hence, there are six possible architectures for the coarse actuators that can achieve the three DOFs for the parallel mechanism as mentioned above. These six architectures are also applied to the fine actuator architectures for each coarse actuator architecture in the same way. Each architecture can be differentiated by the nomenclature as shown in Fig. 2. By using this nomenclature, six types of coarse actuator architectures are represented in Fig. 3. Six types of fine actuator architectures can be obtained by replacing the symbol "C" in Fig. 3 with "F". Thus, the total number of possible coarse-and-fine actuator combinations is 36. For example, some of the coarse-and-fine actuator combinations among the 36 candidates are showed in Fig. 4.

Choosing the proper one among these 36 architectures becomes a major issue at the design process. Because the coarse actuators make the major motion of the mechanism, it is reasonable to select the proper coarse actuator architecture without considering fine actuators in the first step, which will be dealt with in part I of this paper. Then, optimal kinematic parameters will be determined for the selected

https://doi.org/10.1017/S0263574704000396 Published online by Cambridge University Press

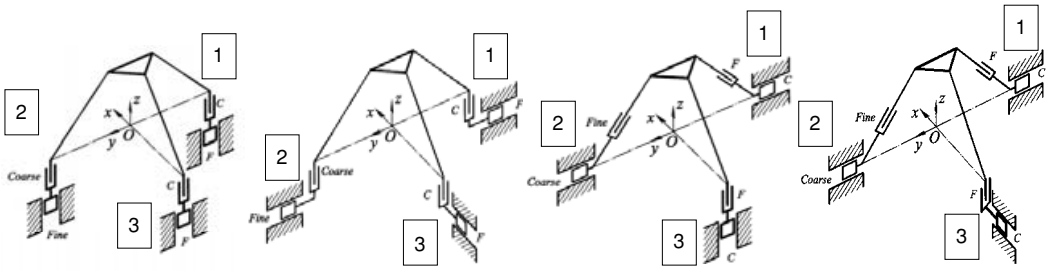


(a) C-VV : F-VV (b) C-VV : F-HH (c) C-HV : F-NV (d) C-HH : F-NV

Fig. 4. Some of the coarse-and-fine actuator combinations.

coarse actuator architecture. After finishing the design of the main coarse actuator architecture, one architecture among these six possible fine actuator architectures will be selected to achieve sub-micron positioning accuracy in part II.

## 3. INVERSE KINEMATICS AND JACOBIAN MATRIX

### *3.1. Inverse kinematics*

The objective of the inverse kinematics solution is to define a mapping from the pose of the output platform in a Cartesian space to the set of actuated inputs that achieve that pose. For this analysis, the pose of the moving platform is considered known, and the position is given by the position vector $(\boldsymbol{O}')_{\Re}$ and the orientation is given by a matrix $\boldsymbol{Q}$. And there are

$$(\boldsymbol{O}')_{\Re} = (x \quad y \quad z)^{\mathrm{T}} \tag{1}$$

where $x = 0$,

$$\boldsymbol{Q} = \begin{bmatrix} \cos\phi & 0 & \sin\phi \\ 0 & 1 & 0 \\ -\sin\phi & 0 & \cos\phi \end{bmatrix} \tag{2}$$

where the angle $\phi$ is the rotational DOF of the output platform with respect to $y$-axis. For the mechanism with C-VV type as shown in Fig. 1, the coordinate of the point $P_i$ in the frame $\Re'$ can be described by the vector $(\boldsymbol{p}_i)_{\Re'}$ $(i = 1, 2, 3)$, and

$$(\boldsymbol{p}_1)_{\Re'} = \begin{pmatrix} 0 \\ -R_1 \\ 0 \end{pmatrix}, \ (\boldsymbol{p}_2)_{\Re'} = \begin{pmatrix} 0 \\ R_1 \\ 0 \end{pmatrix}, \ (\boldsymbol{p}_3)_{\Re'} = \begin{pmatrix} -R_1 \\ 0 \\ 0 \end{pmatrix} \tag{3}$$

Vectors $(\boldsymbol{b}_i)_{\Re}$ $(i = 1, 2, 3)$ will be defined as the position vectors of base joints in frame $\Re$, and

$$(\boldsymbol{b}_1)_{\Re} = \begin{pmatrix} 0 \\ -R_3 \\ Z_{c1} \end{pmatrix}, \ (\boldsymbol{b}_2)_{\Re} = \begin{pmatrix} 0 \\ R_3 \\ Z_{c2} \end{pmatrix}, \ (\boldsymbol{b}_3)_{\Re} = \begin{pmatrix} -R_3 \\ 0 \\ Z_{c3} \end{pmatrix} \tag{4}$$

where $Z_{ci}$ $(i = 1, 2, 3)$ are inputs of the coarse actuators. The vector $(\boldsymbol{p}_i)_{\Re}$ $(i = 1, 2, 3)$ in frame $O$-$xyz$ can be written as

$$(\boldsymbol{p}_i)_{\Re} = \boldsymbol{Q}(\boldsymbol{p}_i)_{\Re'} + (\boldsymbol{O}')_{\Re} \tag{5}$$

Then the inverse kinematics of the parallel manipulator can be solved by writing following constraint equation

$$\|[\boldsymbol{p}_i - \boldsymbol{b}_i]_{\Re}\| = L \quad \text{where } i = 1, 2, 3 \tag{6}$$

Hence, for a given manipulator and for prescribed values of the position and orientation of the platform, the required actuator inputs can be directly computed from Eq. (6), that is

$$Z_{c1} = z \pm \sqrt{L^2 - (y - R_1 + R_3)^2} \tag{7}$$

$$Z_{c2} = z \pm \sqrt{L^2 - (y + R_1 - R_3)^2} \tag{8}$$

$$Z_{c3} = z + R_1 \sin\phi \pm \sqrt{L^2 - y^2 - (-R_1 \cos\phi + R_3)^2} \tag{9}$$

From Eqs. (7), (8) and (9), we can see that there are eight inverse kinematics solutions for a given pose of the parallel manipulator. To obtain the inverse configuration as shown in Fig. 1, each one of the signs "±" in Eqs. (7)∼(9) should be "−".

Following the inverse kinematics analysis for the mechanism with C-VV type, one can obtain the inverse kinematics of the other five types of coarse actuator architectures in the same way. The inverse kinematics solutions for each coarse actuator architecture are derived in Table I. The kinematics of the mechanisms with fine actuators are identical with those with coarse actuators.

### *3.2. Jacobian matrix*

For the mechanism with C-VV type, Eq. (6) can be differentiated with respect to time to obtain the velocity equations, which leads to

$$(z - Z_{c1})\dot{Z}_{c1} = (y - R_1 + R_3)\dot{y} + (z - Z_{c1})\dot{z} \tag{10}$$

$$(z - Z_{c2})\dot{Z}_{c2} = (y + R_1 - R_3)\dot{y} + (z - Z_{c2})\dot{z} \tag{11}$$

$$\begin{aligned}(z - Z_{c3} + R_1 \sin\phi)\dot{Z}_{c3} &= y\dot{y} + (z - Z_{c3} + R_1 \sin\phi)\dot{z} \\ &+ [(z - Z_{c3})R_1 \cos\phi + R_3 R_1 \sin\phi]\dot{\phi}\end{aligned} \tag{12}$$

Rearranging Eqs. (10) ∼(12) leads to an equation of the form

$$\boldsymbol{A}\dot{\boldsymbol{\rho}} = \boldsymbol{B}\dot{\boldsymbol{p}} \tag{13}$$

where $\dot{\boldsymbol{p}}$ is the vector of output velocities defined as

$$\dot{\boldsymbol{p}} = (\dot{y} \quad \dot{z} \quad \dot{\phi})^{\mathrm{T}} \tag{14}$$

and $\dot{\boldsymbol{\rho}}$ is the vector of input velocities defined as

$$\dot{\boldsymbol{\rho}} = (\dot{Z}_{c1} \quad \dot{Z}_{c2} \quad \dot{Z}_{c3})^{\mathrm{T}} \tag{15}$$

https://doi.org/10.1017/S0263574704000396 Published online by Cambridge University Press

Matrices $\boldsymbol{A}$ and $\boldsymbol{B}$ are, respectively, the $3 \times 3$ two separate Jacobian matrices of the manipulator and can be expressed as

$$\boldsymbol{A} = \begin{bmatrix} z - Z_{c1} & 0 & 0 \\ 0 & z - Z_{c2} & 0 \\ 0 & 0 & z - Z_{c3} + R_1 \sin\phi \end{bmatrix} \tag{16}$$

$$\boldsymbol{B} = \begin{bmatrix} y - R_1 + R_3 & z - Z_{c1} & 0 \\ y + R_1 - R_3 & z - Z_{c2} & 0 \\ y & z - Z_{c3} + R_1 \sin\phi & (z - Z_{c3})R_1 \cos\phi + R_3 R_1 \sin\phi \end{bmatrix} \tag{17}$$

The Jacobian matrix $\boldsymbol{J}$ of the manipulator can be obtained as

$$\boldsymbol{J} = \boldsymbol{A}^{-1}\boldsymbol{B} \tag{18}$$

Then, the Jacobian matrices for the six types of architectures with coarse actuators can be written as:

The Jacobian matrices for the six types of architectures with fine actuators can be also obtained by replacing $Z_{ci}$ in Eqs. (19)–(24) with $Z_{fi}$ $(i = 1, 2, 3)$, where $Z_{fi}$ are inputs of the fine actuators.

## 4. SELECTION OF THE COARSE ACTUATOR ARCHITECTURE

A spatial 3-DOF parallel mechanism with a kinematic parameter set of $R_1 = 7.32\,\text{mm}$, $R_3 = 22.5\,\text{mm}$ and $L = 23.93\,\text{mm}$ is used to evaluate six possible coarse actuator architectures. The workspace of this parallel mechanism is selected as $y \in [-\frac{R_1}{2}, +\frac{R_1}{2}] = [-3.66\,\text{mm}, +3.66\,\text{mm}]$ and $z \in [0.0, 5.00\,\text{mm}]$. Actually this kinematic parameter set is the optimal design result, which will be discussed in part II.

### *4.1. Mobility analysis*

An important factor that should be considered in the design of our mechanism is the evaluation of the rotational capability of the moving platform (defined as mobility here) at a point in the workspace. Usually the parallel mechanisms such as the

$$\boldsymbol{J}_{VV} = \begin{bmatrix} z - Z_{c1} & 0 & 0 \\ 0 & z - Z_{c2} & 0 \\ 0 & 0 & z - Z_{c3} - R_1 \sin\phi \end{bmatrix}^{-1} \begin{bmatrix} y - R_1 + R_3 & z - Z_{c1} & 0 \\ y + R_1 - R_3 & z - Z_{c2} & 0 \\ y & z - Z_{c3} + R_1 \sin\phi & (z - Z_{c3})R_1 \cos\phi + R_3 R_1 \sin\phi \end{bmatrix} \tag{19}$$

$$\boldsymbol{J}_{VH} = \begin{bmatrix} z - Z_{c1} & 0 & 0 \\ 0 & z - Z_{c2} & 0 \\ 0 & 0 & R_3 - Z_{c3} - R_1 \cos\phi \end{bmatrix}^{-1} \begin{bmatrix} y - R_1 + R_3 & z - Z_{c1} & 0 \\ y + R_1 - R_3 & z - Z_{c2} & 0 \\ y & z + R_1 \sin\phi & zR_1 \cos\phi + (R_3 - Z_{c3})R_1 \sin\phi \end{bmatrix} \tag{20}$$

$$\boldsymbol{J}_{HV} = \begin{bmatrix} y - Z_{c1} - R_1 + R_3 & 0 & 0 \\ 0 & y - Z_{c2} + R_1 - R_3 & 0 \\ 0 & 0 & z - Z_{c3} + R_1 \sin\phi \end{bmatrix}^{-1} \times \begin{bmatrix} y - Z_{c1} - R_1 + R_3 & z & 0 \\ y - Z_{c2} + R_1 - R_3 & z & 0 \\ y & z - Z_{c3} + R_1 \sin\phi & (z - Z_{c3})R_1 \cos\phi + R_3 R_1 \sin\phi \end{bmatrix} \tag{21}$$

$$\boldsymbol{J}_{HH} = \begin{bmatrix} y - Z_{c1} - R_1 + R_3 & 0 & 0 \\ 0 & y - Z_{c2} + R_1 - R_3 & 0 \\ 0 & 0 & R_3 - Z_{c3} - R_1 \cos\phi \end{bmatrix}^{-1} \times \begin{bmatrix} y - Z_{c1} - R_1 + R_3 & z & 0 \\ y - Z_{c2} + R_1 - R_3 & z & 0 \\ y & z + R_1 \sin\phi & zR_1 \cos\phi + (R_3 - Z_{c3})R_1 \sin\phi \end{bmatrix} \tag{22}$$

$$\boldsymbol{J}_{NV} = \begin{bmatrix} L + Z_{c1} & 0 & 0 \\ 0 & L + Z_{c2} & 0 \\ 0 & 0 & z - Z_{c3} + R_1 \sin\phi \end{bmatrix}^{-1} \times \begin{bmatrix} y - R_1 + R_3 & z & 0 \\ y + R_1 - R_3 & z & 0 \\ y & z - Z_{c3} + R_1 \sin\phi & (z - Z_{c3})R_1 \cos\phi + R_3 R_1 \sin\phi \end{bmatrix} \tag{23}$$

$$\boldsymbol{J}_{NH} = \begin{bmatrix} L + Z_{c1} & 0 & 0 \\ 0 & L + Z_{c2} & 0 \\ 0 & 0 & R_3 - Z_{c3} - R_1 \cos\phi \end{bmatrix}^{-1} \begin{bmatrix} y - R_1 + R_3 & z & 0 \\ y + R_1 - R_3 & z & 0 \\ y & z + R_1 \sin\phi & zR_1 \cos\phi + (R_3 - Z_{c3})R_1 \sin\phi \end{bmatrix} \tag{24}$$

https://doi.org/10.1017/S0263574704000396 Published online by Cambridge University Press

Table I. Inverse kinematic solutions for six coarse actuator architectures.

| Type | Inverse kinematic solutions |
|---|---|
| C-VV | $Z_{c1} = z \pm \sqrt{L^2 - (y - R_1 + R_3)^2}$, $Z_{c2} = z \pm \sqrt{L^2 - (y + R_1 - R_3)^2}$, $Z_{c3} = z + R_1 \sin\phi \pm \sqrt{L^2 - y^2 - (-R_1 \cos\phi + R_3)^2}$ |
| C-VH | $Z_{c1} = z \pm \sqrt{L^2 - (y - R_1 + R_3)^2}$, $Z_{c2} = z \pm \sqrt{L^2 - (y + R_1 - R_3)^2}$, $Z_{c3} = -R_1 \cos\phi + R_3 \pm \sqrt{L^2 - y^2 - (z + R_1 \sin\phi)^2}$ |
| C-HV | $Z_{c1} = y - R_1 + R_3 \pm \sqrt{L^2 - z^2}$, $Z_{c2} = y + R_1 - R_3 \pm \sqrt{L^2 - z^2}$, $Z_{c3} = z + R_1 \sin\phi \pm \sqrt{L^2 - y^2 - (-R_1 \cos\phi + R_3)^2}$ |
| C-HH | $Z_{c1} = y - R_1 + R_3 \pm \sqrt{L^2 - z^2}$, $Z_{c2} = y + R_1 - R_3 \pm \sqrt{L^2 - z^2}$, $Z_{c3} = -R_1 \cos\phi + R_3 \pm \sqrt{L^2 - y^2 - (z + R_1 \sin\phi)^2}$ |
| C-NV | $Z_{c1} = -L \pm \sqrt{(y - R_1 + R_3)^2 + z^2}$, $Z_{c2} = -L \pm \sqrt{(y + R_1 - R_3)^2 + z^2}$, $Z_{c3} = z + R_1 \sin\phi \pm \sqrt{L^2 - y^2 - (-R_1 \cos\phi + R_3)^2}$ |
| C-NH | $Z_{c1} = -L \pm \sqrt{(y - R_1 + R_3)^2 + z^2}$, $Z_{c2} = -L \pm \sqrt{(y + R_1 - R_3)^2 + z^2}$, $Z_{c3} = -R_1 \cos\phi + R_3 \pm \sqrt{L^2 - y^2 - (z + R_1 \sin\phi)^2}$ |

Stewart-Gough platforms have lower mobility, which limits further applications in the industry.[6] One of the purposes of this new design is to develop a parallel mechanism that has the mobility with 100° tilting angle. Therefore, each coarse actuator architecture should be confirmed as to whether it has the mobility of more than 100° tilting angle.

Before discussing the mobility, the singularity must be considered because it affects the mobility of the parallel mechanism. As analyzed by Liu *et al*,[11] there are three kinds of singularities, which can be obtained from the matrices $\boldsymbol{A}$ and/or $\boldsymbol{B}$ in Eq. (13). The first kind of singularity corresponds to the configuration in which the chain reaches either a boundary of its workspace or an internal boundary limiting different sub-regions of the workspace. This type of configuration for the mechanism is reached whenever one of $P_1B_1$, $P_2B_2$, and $P_3B_3$ is in the plane perpendicular to each slider axis attached to the base connecting each leg to the base. In the second kind of singular configuration, the output link is locally movable even when all the actuated joints are locked. The singularity will occur when the third leg $P_3B_3$ is in the plane defined by $P_1$, $P_2$ and $P_3$. The third kind of singularity is the architecture singularity. For the parallel mechanism concerned in this paper, either $R_3 = R_1 + L$ or $R_3 = R_1$ will lead to this type of singularity. Actually, to design our mechanism, the first and second kinds of singularities within the workspace are worth considering. Fig. 5 shows the singular positions at $O'$(0,0,0) for the six coarse actuator architectures where the singular angles of the platform with respect to the horizontal $O$-$xy$ plane are $\phi = 101.27°$ (the first kind of singularity), $-43.95°$ (the second kind of singularity) for the vertical types in the 3rd leg (VV, HV, and NV types) and $\phi = -227.89°$ (the first kind of singularity), $\phi = -36.30°$ (the second kind of singularity) for the horizontal types in the 3rd leg (VH, HH, and NH types). This condition will limit the mobility of the parallel mechanism.

According to the kinematics of the 3-DOF parallel mechanism, the rotational DOF is the rotation of the moving platform with respect to $y$-axis. To evaluate this mobility, local mobility (*LM*) is introduced as shown in Fig. 6. Local mobility is defined as the maximum rotational angle of the platform that does not have any singularity within the kinematic compatibility range or actuator travel range. Here the kinematic compatibility range means the range where inverse kinematic solutions exist. Global mobility is defined as the maximum rotational angle of the platform within the kinematic compatibility range or actuator travel range. Global mobility (*GM*) does not consider singularity, which will separate the arc into two inaccessible ones as shown in Fig. 6. Real mechanisms cannot pass the singularity positions so they should be remained one of the two arcs, and each arc can be defined as local mobility as above. Note that we will only consider the kinematic compatibility assuming that the actuator travel range is limitless when evaluating the mobility in this section.

The movement of the third leg mainly makes the rotational DOF motion about $y$-axis. Hence, even if we have six possible coarse actuator architectures, the trend in the mobility of each architecture is divided into two categories according to the positions of the third leg coarse actuators. For example, the mobility for six possible coarse actuator architectures at the home position $O'$(0,0,0) is calculated as shown in Fig. 7 where the vertical types in the 3rd leg (VV, HV, and NV types) have the local mobility of 145.21° and the horizontal types in the 3rd leg (VH, HH, and NH types) have the local mobility of 191.59°. According to these results obtained using the home position, all types satisfy the mobility of more than 100°.

The local mobility distribution for the whole workspace is calculated as shown in Fig. 8. The vertical types in the 3rd leg (VV, HV, and NV types) have the same mobility along the $z$ coordinates of the platform for a given $y$ coordinate of

https://doi.org/10.1017/S0263574704000396 Published online by Cambridge University Press

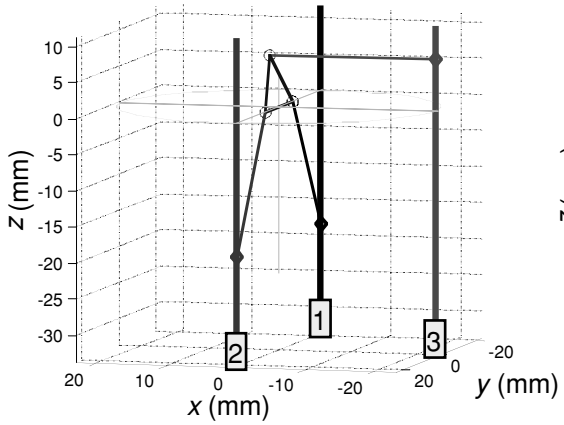


(a) The first kind of singularity, $\phi$ = 101.27°, for vertical types

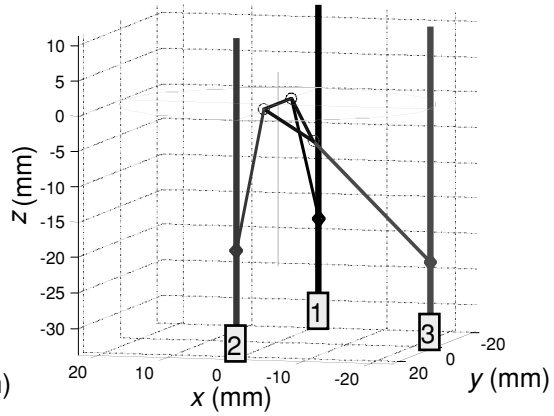


(b) The second kind of singularity, $\phi$ = -43.95°, for vertical types

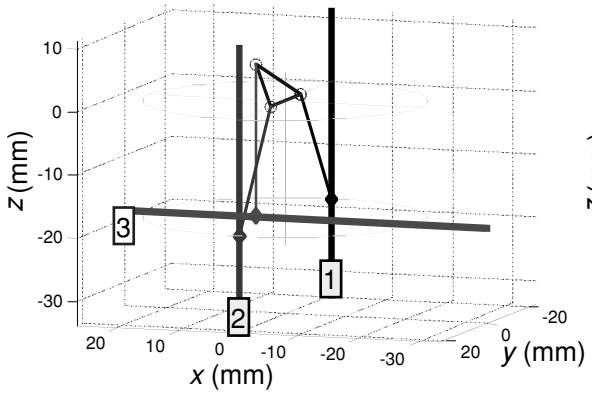


(c) The first kind of singularity, $\phi$ = -227.89°, for horizontal types

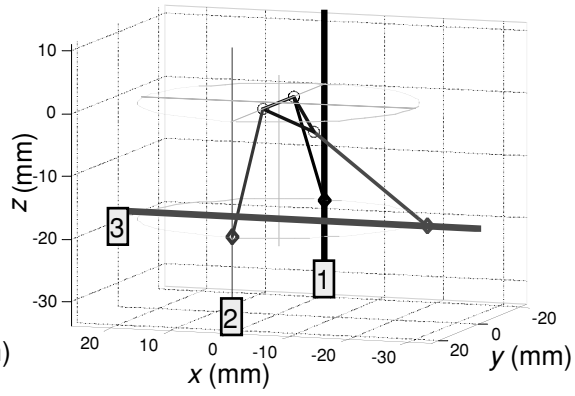


(d) The second kind of singularity, $\phi$ = -36.30°, for horizontal types

Fig. 5. Singularity at $O'$(0,0,0) for the third leg.

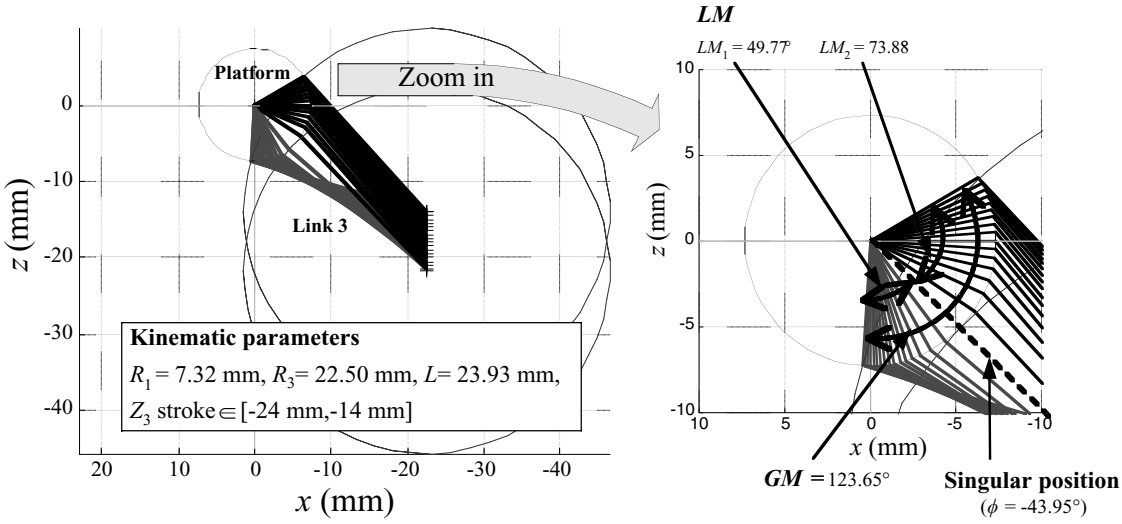


Fig. 6. Definition of global mobility (*GM*) and local mobility(*LM*) at $O'$(0,0,0).

https://doi.org/10.1017/S0263574704000396 Published online by Cambridge University Press

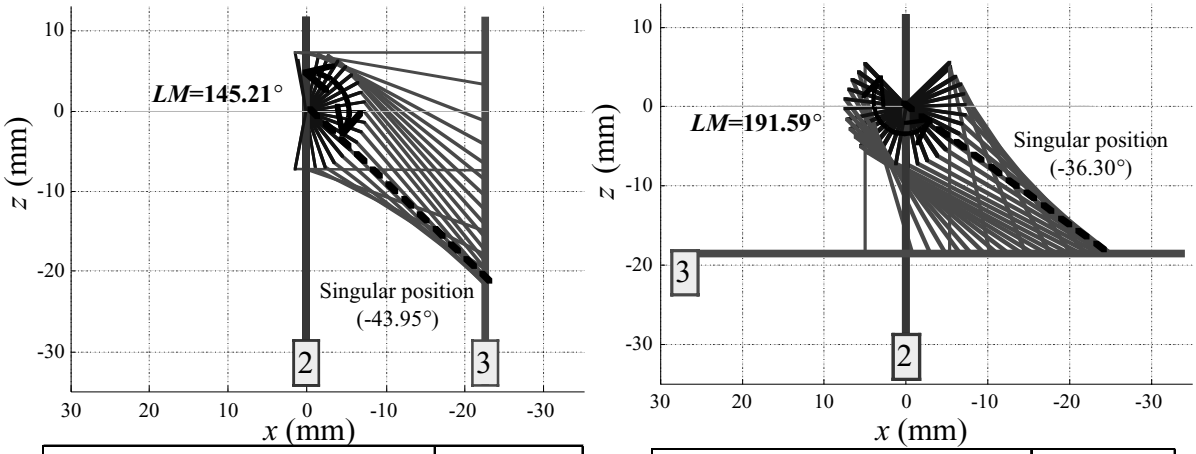


| Properties | | Angle(°) |
|---|---|---|
| *GM* | Lower limit | -101.27 |
| | Upper limit | 101.27 |
| | *GM* | **202.54** |
| *LM* | Lower(Singular) | -43.95 |
| | Upper limit | 101.27 |
| | *LM* | **145.21** |

(a) Vertical type in the 3rd leg (VV, HV, NV)

| Properties | | Angle(°) |
|---|---|---|
| *GM* | Lower limit | -227.89 |
| | Upper limit | 47.89 |
| | *GM* | **275.77** |
| *LM* | Lower limit | -227.89 |
| | Upper(Singular) | -36.30 |
| | *LM* | **191.59** |

(b) Horizontal type in the 3rd leg (VH, HH, NH)

Fig. 7. Local mobility at $O'(0,0,0)$ for the six coarse actuator architectures.

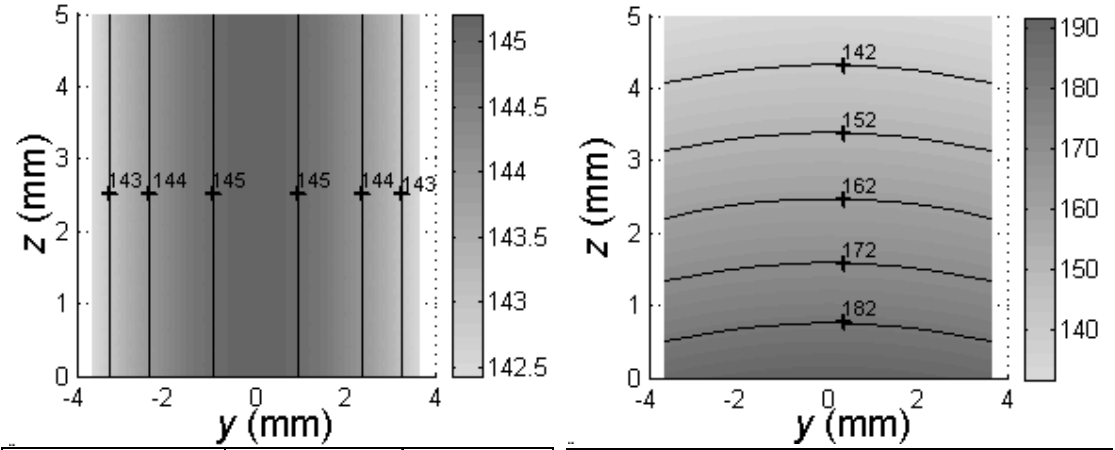


| *LM* | Maximum(°) ($y$=0) | Minimum(°) ($y$=+/- 3.66) |
|---|---|---|
| Lower(Singular) limit | -43.95 | -43.40 |
| Upper limit | 101.27 | 99.03 |
| ***LM*** | **145.22** | **142.43** |

(a) Vertical type in 3rd leg (VV, HV, NV)

| *LM* | Maximum(°) ($y$=0, $z$=0) | Minimum(°) ($y$=+/-3.66, $z$=5) |
|---|---|---|
| Lower limit | -227.89 | -181.16 |
| Upper(Singular) limit | -36.30 | -49.36 |
| ***LM*** | **191.59** | **131.80** |

(b) Horizontal type in 3rd leg (VH, HH, NH)

Fig. 8. Local mobility (*LM*) distribution within the whole workspace.

the platform. For each of these types, the maximum local mobility is 145.22° when $y = 0$ and the minimum local mobility is 142.43° when $y = \pm 3.66$ mm. For each of the horizontal types in the 3rd leg (VH, HH, and NH types), the maximum local mobility is 191.59° when $O'(0,0,0)$ and the minimum local mobility is 131.80° when $O'(0, \pm 3.66\,\text{mm}, 5.0\,\text{mm})$. From these results we can guarantee that the mobility requirement (>100°) is satisfied for all six possible coarse actuator architectures.

### *4.2. Conditioning index analysis*

The kinematic performance of a mechanism is closely related to the numerical stability of the mapping from platform velocity to joint velocity. The Jacobian matrix usually describes this mapping. Thus the kinematic performance of a mechanism is closely related to the numerical condition of its Jacobian matrix.

In the problem of mechanism designs, some kinematic performance indices based on the Jacobian matrix have been

https://doi.org/10.1017/S0263574704000396 Published online by Cambridge University Press

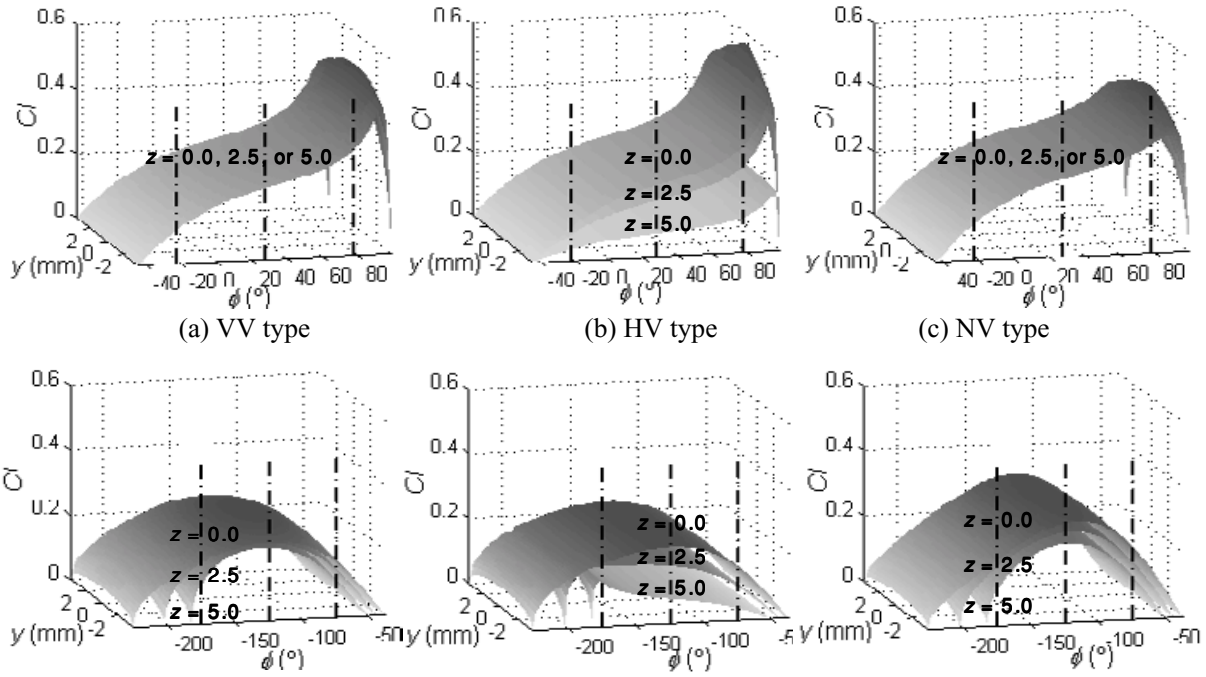


(a) VV type (b) HV type (c) NV type

(d) VH type (e) HH type (f) NH type

Fig. 9. *CI* distributions at $z = 0.0$, 2.5 mm and 5.0 mm for the six coarse actuator architectures.

proposed.[12] Among these indices, the condition number of the Jacobian matrix seems to be the most favorable one because the condition number is considered as a measure of the kinematic accuracy and the proximity to singularity of a mechanism. The condition number $\kappa$ is defined as the ratio of the maximum singular value of the Jacobian matrix and the minimum one as follows,

$$\kappa = \|\boldsymbol{J}^{-1}\| \cdot \|\boldsymbol{J}\|, \quad \text{and} \quad 1 \leq \kappa < \infty \tag{25}$$

where $\|\cdot\|$ denotes any norm of a matrix. As $\kappa$ approaches unity, the resulting mechanism becomes kinematically more isotropic and as it moves away form unity, the mechanism gets closer to a singular position. So, it is better to have a condition number that is as small as possible because it ensures that the error on the actuated joints affects the moving platform position as little as possible.[7]

For evaluating the condition number for the six possible coarse actuator architectures, the conditioning index (*CI*) is defined as the reciprocal of the condition number of the Jacobian matrix, i.e.

$$CI = \frac{1}{\kappa}, \quad \text{and} \quad 0 \leq CI \leq 1 \tag{26}$$

The reason for using the *CI* instead of the condition number itself is that the *CI* is bounded within 0 to 1, and hence, is very convenient to handle. The condition number, on the contrary, becomes infinity at singularities and hence, produces numerical overflows. When evaluating the *CI*, it is better to have the *CI* that is near one, which means it has less amplification of the errors between the joint space and the Cartesian space and it is far from singularity.

As pointed out by H. Lipkin and J. Duffy,[13] the condition number of the Jacobian matrix is of little practical significance in the presence of non-uniform physical units which appear when a mechanism can both translate and rotate its end-effector like our mechanism. The matrix $\boldsymbol{A}$ of Eq. (18) has no problem with the dimensional inhomogeneity. But the matrix $\boldsymbol{B}$ of Eq. (18) is not dimensionally homogeneous for its first two columns have units of length, while its third column has units of length-squared. To overcome this problem we can redefine the matrix $\boldsymbol{B}$ by invoking the concept of characteristic length which can be defined in many ways depending on individual's interest.[14] To render $\boldsymbol{B}$ dimensionally homogeneous we divide the third column of $\boldsymbol{B}$ by $R_2$. An additional parameter $R_2$, which is the vertical distance between the origin of the moving platform and the 1st or 2nd base joint (that is, the distance between lines $P_1P_2$ and $B_1B_2$ in Fig. 1) at the home position $O'(0,0,0)$, is introduced. There is a relation of $L = \sqrt{(R_3 - R_1)^2 + R_2^2}$ between kinematic parameters. We choose $R_2$ as the characteristic length because it represents typical height of the mechanism at the home position and it has combined relation between parameters.

The *CI* distributions at $z = 0.0$, 2.5 mm, and 5.0 mm within the workspace for the six possible coarse actuator architectures are displayed in Fig. 9. For the HV and HH types, the CI values are varied along the $z$ coordinates of the platform and become lower than other types when $z = 5.0$ mm, therefore, these two types can be excluded in the selection. For the VH and NH types, the *CI* values are relatively high although they are varied along the $z$ coordinates of the platform. For the VV and NV types, the *CI* values are relatively high and almost same along the $z$ coordinates of the platform.

To compare accurately and obtain a measure of the global behavior of the manipulator condition number over the 100°

https://doi.org/10.1017/S0263574704000396 Published online by Cambridge University Press

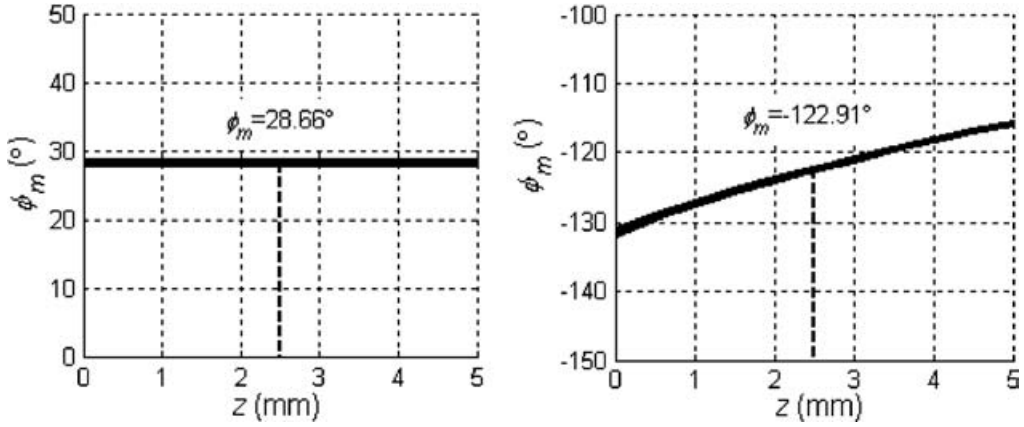


(a) Vertical type in 3rd leg (VV, HV, NV) (b) Horizontal type in 3rd leg (VH, HH, NH)

Fig. 10. Middle angle ($\phi_m$) distributions along the $z$ directional workspace.

tilting range, *GMCI* (Global Mobility Conditioning Index) is defined as

$$GMCI = \frac{\int_{\phi_m-50^\circ}^{\phi_m+50^\circ} \frac{1}{\kappa} d\phi}{\int_{\phi_m-50^\circ}^{\phi_m+50^\circ} d\phi}, \quad \text{and} \quad 0 < GMCI < 1 \qquad (27)$$

where $\phi_m$ is the average value of the middle angles of the local mobility along the $z$ directional workspace (5 mm) for each coarse actuator architecture. As shown in Fig. 7 tilting ranges are different depending on the types of architectures. In order to compare the conditioning indices fairly considering 100° tilting range we should find out proper representative tilting range for each type of architecture. So the average value of the middle angles of the local mobility along the $z$ directional workspace $\phi_m$ and the integral interval $[\phi_m - 50^\circ, \phi_m + 50^\circ]$ are selected to represent 100° tilting range for each type of architecture. In Fig. 9, the middle line among three vertical dash lines in each figure represents $\phi_m$ and the other two lines represent the 100° tilting range of $[\phi_m - 50^\circ, \phi_m + 50^\circ]$. As shown in Fig. 10, $\phi_m = 28.66^\circ$ for the vertical types in the 3rd leg (VV, HV, and NV types) and $\phi_m = -122.91^\circ$ for the horizontal types in the 3rd leg (VH, HH, and NH types). *GMCI* represents the average *CI* value of one position in the workspace for 100° tilt. As the *CI* is bounded within 0 to 1 as shown in Eq. (26), *GMCI* produces a bounded performance index, i.e., $0 < GMCI < 1$. Larger *GMCI* is preferred because the closer to unity the index is, the better the overall behavior of the conditioning index over the 100° tilting range of $[\phi_m - 50^\circ, \phi_m + 50^\circ]$ is.

Fig. 11 shows the distributions of the *GMCI* within the workspace for the six possible coarse actuator architectures. The average of *GMCI* within the workspace for each coarse actuator architecture is also shown in Fig. 11.

The HV and HH types are worst as confirmed from Fig. 9 because they have low *CI* values and approaches singularity in some positions. The variable link types (NV and NH types) have better *CI* values but considering the manufacture of small-sized components, small variable links with built-in prismatic actuators are very difficult to make. Thus, besides the NV and NH types, we conclude that the VV type coarse actuator architecture is the proper choice because it has the best *GMCI* value. The VV type has another advantage in that

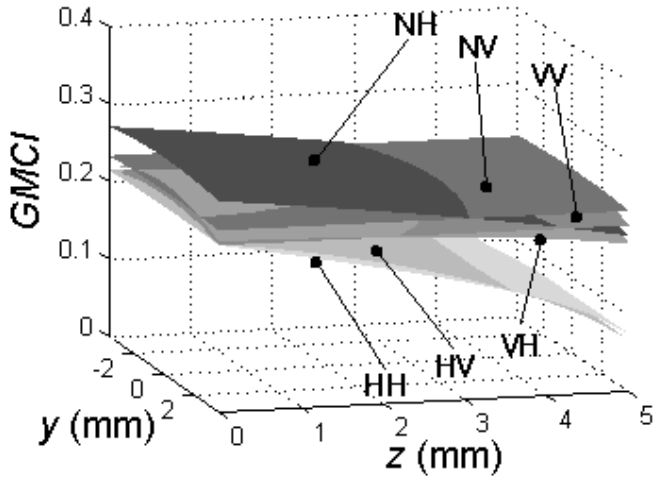


| Types | *GMCI* average | Place |
|---|---|---|
| NH | 0.2460 | 1 |
| NV | 0.2373 | 2 |
| VV | 0.2268 | 3 |
| VH | 0.2259 | 4 |
| HV | 0.1620 | 5 |
| HH | 0.1603 | 6 |

Fig. 11. *GMCI* distribution within the workspace for the six possible architectures with coarse actuators.

https://doi.org/10.1017/S0263574704000396 Published online by Cambridge University Press

the *CI* values are same with $z$ coordinate variation of the platform for a given $y$ coordinate of the platform.

## 5. CONCLUSIONS

This paper proposes a new design for the micro parallel positioning platform with high mobility, high accuracy, and a large working space by using the dual stage system. The positioning platform is based on a new spatial 3-DOF parallel mechanism which has a distinct advantage in high mobility. The parallel mechanism has spatial three DOFs of two translations and one rotation. The dual stage system with the coarse and fine actuators is adopted to achieve sub-micron accuracy with a large working space. The coarse actuator offers a large working space and actuation powers, while the fine actuator enables high resolution of motion.

To achieve these three DOFs and implement the dual stage system in the parallel mechanism, there are six possible architectures for the coarse and fine actuators, respectively. In part I, inverse kinematics and Jacobian matrices for six types of coarse actuator architecture are derived. And the C-VV type is selected for the coarse actuator architecture after evaluating six coarse actuator architectures by the criteria of the mobility of more than 100°, better condition number of the Jacobian matrix, and manufacturability consideration. Optimal design for the selected coarse actuator architecture and selection of fine actuator architecture are discussed in part II (next issue of *Robotica*).

## Acknowledgement

This work was supported by the NRL Program on Next Generation Parallel Mechanism Platforms and partly by the Micro-thermal System ERC and the Brain Korea 21 Project in 2003.

## References

1. N. Kawahara, T. Suto, T. Hirano, Y. Ishikawa, T. Kitahara, N. Ooyama and T. Ataka, "Microfactories; new applications of micromachine technology to the manufacture of small products," *Microsystem Technologies* **3**(2), 37–41 (1997).
2. H. Liu, B. Lu, Y. Ding, Y. Tang and D. Li, "A motor-piezo actuator for nano-scale positioning based on dual servo loop and nonlinearity compensation," *Journal of Micromechanics and Microengineering* **13**, 295–299 (2003).
3. H. J. Pahk, D. S. Lee and J. H. Park, "Ultra precision positioning system for servo motor-piezo actuator using the dual servo loop and digital filter implementation," *International Journal of Machine Tools and Manufacture* **41**(1), 51–63 (2001).
4. S. Kwon, W. K. Chung and Y. Youm, "On the coarse/fine dual-stage manipulators with robust perturbation compensator," *Proceedings of the 2001 IEEE International Conference on Robotics and Automation*, Seoul, Korea (May 21–26, 2001) pp. 121–126.
5. E. Pernette, S. Henein, I. Magnani and R. Clavel, "Design of parallel robots in microrobotics," *Robotica* **15**(4), 417–420 (1997).
6. M. Weck and D. Staimer, "Parallel kinematic machine tools – Current state and future potentials," *CIRP Annals Manufacturing Technology* **51**, 671–683 (2002).
7. J. P. Merlet, *Parallel Robots*, Solid mechanics and its applications **Vol. 74** (Kluwer Academic Publishers, Dordrecht, The Netherlands, 2000).
8. S. H. Chang, C. K. Tseng and H. C. Chien, "An Ultra-Precision XYQz Piezo-Micropositioner Part I: Design and analysis," *IEEE Transactions on Ultrasonics, Ferroelectrics, and Frequency Control* **46**(4), 897–905 (1999).
9. G. B. Chung, B.-J. Yi, I. H. Suh, W. K. Kim and W. K. Chung, "Design and analysis of a spatial 3-DOF micromanipulator for tele-operation," *Proceedings of the 2001 IEEE/RSJ International Conference on Intelligent Robots and Systems*, Maui, Hawaii, USA (Oct. 29∼Nov. 03, 2001) pp. 337–342.
10. Y. Takeda, K. Ichikawa, H. Funabashi and K. Hirose, "A Spatial Six-DOF Hybrid In-Parallel Actuated Mechanism for Fine Postitioning Within a Large Working Space," *Proceedings of the The 1st Korea-Japan Conference on Positioning Technology* (CPT2002), Daejeon, Korea (October 15–17, 2002) pp. 141–146.
11. X.-J. Liu, J. Wang, F. Gao and L.-P. Wang, "On the analysis of a new spatial three-degrees-of-freedom parallel manipulator," *IEEE Transactions on Robotics and Automation* **17**, 959–968 (2001).
12. S. Khatami and F. Sassani, "Isotropic design optimization of robotic manipulators using a genetic algorithm method," *Proceedings of the 2002 IEEE International Symposium on Intelligent Control* (October 27–30, 2002) pp. 562–567.
13. H. Lipkin and J. Duffy, "Hybrid Twist and Wrench Control for a Robotic Manipulator," *Journal of Mechanisms, Transmissions, and Automation in Design* **110**(2), 138–144 (1988).
14. O. Ma and J. Angeles, "Optimum architecture design of platform manipulators," *Proceedings of the Fifth International Conference on Advanced Robotics*, Pisa, Italy (19–22 June, 1991) pp. 1130–1135.